HHS Public Access

Author manuscript

IEEE Trans Biomed Eng. Author manuscript; available in PMC 2016 September 01.

Published in final edited form as:

IEEE Trans Biomed Eng. 2015 September ; 62(9): 2177–2186. doi:10.1109/TBME.2015.2415731.

Patient Registration Using Intraoperative Stereovision in Image-guided Open Spinal Surgery

Songbai Ji,
Thayer School of Engineering, Dartmouth, Hanover, NH 03755 USA

Xiaoyao Fan,
Thayer School of Engineering, Dartmouth, Hanover, NH 03755 USA

Keith D. Paulsen [Senior Member IEEE],
Thayer School of Engineering, Dartmouth, Hanover, NH 03755 USA

David W. Roberts,
Geisel School of Medicine, Dartmouth College, Hanover NH 03755, USA, and with Dartmouth Hitchcock Medical Center, Lebanon NH 03766 USA

Sohail K. Mirza, and
Geisel School of Medicine, Dartmouth College, Hanover NH 03755, USA, and with Dartmouth Hitchcock Medical Center, Lebanon NH 03766 USA

S. Scott Lollis
Geisel School of Medicine, Dartmouth College, Hanover NH 03755, USA, and with Dartmouth Hitchcock Medical Center, Lebanon NH 03766 USA

Songbai Ji: Songbai.Ji@dartmouth.edu; Xiaoyao Fan: Xiaoyao.Fan@dartmouth.edu; Keith D. Paulsen: Keith.D.Paulsen@dartmouth.edu; David W. Roberts: David.W.Roberts@hitchcock.org; Sohail K. Mirza: Sohail.K.Mirza@hitchcock.org; S. Scott Lollis: S.Scott.Lollis@hitchcock.org

Abstract

Despite its widespread availability and success in open cranial neurosurgery, image-guidance technology remains more limited in use in open spinal procedures, in large part because of patient registration challenges. In this study, we evaluated the feasibility of using intraoperative stereovision (iSV) for accurate, efficient and robust patient registration in open spinal fusion surgery. Geometrical surfaces of exposed vertebrae were first reconstructed from iSV. A classical multi-start registration was then executed between point clouds generated from iSV and preoperative CT (pCT) images of the spine. With two pairs of feature points manually identified to facilitate the registration, an average registration accuracy of 1.43 mm in terms of surface-to-surface distance error was achieved in 8 patient cases using a single iSV image pair sampling 2–3 vertebral segments. The iSV registration error was consistently smaller than the conventional landmark approach for every case (average of 2.02 mm with the same error metric). The large capture ranges (average of 23.8 mm in translation and 46.0 deg in rotation) found in the iSV patient registration suggest the technique may offer sufficient robustness for practical application

Correspondence to: Songbai Ji, Songbai.Ji@dartmouth.edu.

in the operating room. Although some manual effort was still necessary, the manually-derived inputs for iSV registration only needed to be approximate as opposed to be precise and accurate for the manual efforts required in landmark registration. The total computational cost of the iSV registration was 1.5 min on average, significantly less than the typical ~30 min required for the landmark approach. These findings support the clinical feasibility of iSV to offer accurate, efficient and robust patient registration in open spinal surgery, and therefore, its potential to further increase the adoption of image-guidance in this surgical specialty.

Index Terms

Fusion surgery; intraoperative stereovision; patient registration; registration accuracy; spinal surgery

I. Introduction

Despite its widespread commercial availability and success in cranial neurosurgery, use of image-guidance Most spinal applications have involved a narrow set of clinical indications such as fusion and stereotactic radiation delivery, and image-guidance has remained largely unrealized in tumor removal, assessment of deformity correction, or even simpler surgeries such as decompression and discectomy. Even in the area of spinal fusion, 60% of surgeons never use image guidance, while only 11% of spine surgeons employ the technique on a regular basis [3].

For spinal fusion procedures in which pedicle screws are implanted to stabilize vertebral instabilities resulting from disk degeneration, congenital deformities, and trauma [4], the accuracy of screw insertion is critical. Unfortunately, failure or “misplacement” rates of pedicle screw insertion can be as high as 30% in the lumbar spine or even 55% in the thoracic region, when using conventional free-hand techniques [5]; higher misplacement rates in the thoracic spine are likely due to the smaller anatomic confinements of the pedicle in this area. While most pedicle breaches are asymptomatic, screw misplacement can result in impingement on a nerve (causing pain or neurologic deficit), injury to the dura or the spinal cord (leading to cerebrospinal fluid leakage or permanent paralysis), and in rare cases, injury to a major artery or vein (a potentially fatal complication) [6]–[8].

The use of image guidance improves surgical accuracy. Numerous studies have shown that use of image-guidance is associated with a decreased incidence in screw misplacement, compared to the conventional free-hand approach, especially when using navigational systems based on computed tomography (CT) or three-dimensional (3D) fluoroscopy [2], [5], [9]–[12]. A randomized, controlled trial of navigated vs. freehand pedicle screw insertion found a substantial, statistically significant reduction of pedicle breach with navigation (2% vs 23%, [13]). While no study has confirmed superior clinical outcomes with the use of intra-operative navigation, the relative rarity of neurologic or vascular injury and the challenge of accruing a cohort with sufficient statistical power are practical barriers to completion of a randomized trial.

Resistance to a wider acceptance of spinal image-guidance technology is largely due to the inefficiency of patient registration, which is a process to establish the spatial transformation between preoperative images and the patient's anatomy in the operating room (OR). In cranial neurosurgery, the scalp's relative immobility enables the use of skin fiducials for simple, accurate, and quick registration. However, the soft tissues over the spine are mobile; therefore, skin fiducials are not a viable option for spinal surgery. When skin fiducials have been used, large registration errors have been reported (up to 2 cm [14] or even 3 cm at the level of the disc space [15]). Instead, spinal registration typically involves identification of anatomic landmarks within the surgical field. This requires a substantial investment in time and effort on the part of the surgeon to define, expose, and localize these locations [16]. Moreover, the one-time registration at the start of surgery cannot account for intervertebral motion that occurs after surgery is begun. Spinal surgery is a physical process, requiring large-excursion surgical manipulation for bone removal and screw placement. This intra-operative movement degrades navigational accuracy, especially when multiple vertebrae are involved. Although guidance is attainable directly from images acquired with intraoperative CT (iCT) and 2D or 3D fluoroscopy, radiation exposure (occupational and medical) from these techniques is a concern, and their substantial capital costs are additional barriers to wider deployment.

Radiation-free intraoperative images from ultrasound (US; [17]–[22]), stereovision (iSV; [23]–[25]), laser range scanning (LRS) [26], [27], and more recently, conoscopic holography [28] have been employed to aid navigation in image-guided surgical interventions. Both feature- and intensity-based methods can be used to register US with CT of the spine. With a feature-based approach, contours of bony surfaces in US and CT are registered via the iterative closest point (ICP; [29]) technique [18] or more recent variations that improve the registration algorithm efficiency, robustness and tolerance of noise and poor initial starting positions [30]. However, because registration performance depends on accurate feature segmentation in US, which is often manual, its utility is limited in practice. Intensity-based US-to-CT registration eliminates manual segmentation, but typically requires image preprocessing to increase the similarity of bony features in US and CT before the registration begins [19]–[22].

Vision-based intraoperative images [31] including iSV and LRS capture 3D geometry and texture intensity of the exposed anatomical surface. They have been successfully employed to register either with preoperative magnetic resonance images of the brain [26], [27], [32], [33] or with each other, when acquired at two temporally distinct surgical stages [24], [27], [34], [35], to compensate for intraoperative brain shift. Because reconstructed stereoscopic surfaces provide both 3D geometry and texture intensity, either source of information can be employed for registration separately or in combination. Rigid registrations that depend solely on geometry (e.g., via ICP [29]) may not be sufficiently accurate especially when significant lateral brain shift occurs [36]. In this case, incorporating both 3D geometry and texture intensity improves registration accuracy [24]. On the other hand, when registering two textured 3D surfaces acquired with iSV or LRS at two different points in time, the 3D surfaces can be projected into a common 2D coordinate system to transform the 3D geometrical surface registration problem into a simpler 2D image registration [34], [35]. This concept is especially appealing in clinical applications where the registration process

needs to be fully automated, and can be achieved with optical-flow-based registration of the iSV images [35] without requiring manual feature segmentation (e.g., vessels [27]).

Despite these effective and substantial deployments in cranial neurosurgery [31], vision-based guidance techniques have not been applied to open spinal surgery to date [2]. The primary purpose of this study is to evaluate the performance of the iSV methods we previously developed in the setting of image-guided cranial surgery [35], [37], for rapid intraoperative patient registration in open spinal fusion procedures with minimal user intervention. The efforts provide insight into the clinical feasibility of using this radiation-free, noninvasive imaging technique as the basis for establishing accurate, efficient and robust image-guidance and navigation during spinal fusions.

II. Methods

A. Patient cases and anatomical landmark registration

Eight patients undergoing open spinal fusion surgeries were prospectively recruited under the approval from the Dartmouth Institutional Review Board. Patient demographic information is summarized in Table I. For each patient, preoperative CT (pCT) images of the spine were acquired in the standard supine position. Anatomical landmarks (e.g., tips of the transverse and spinous processes) were manually identified in pCT during planning prior to surgery. After opening the spine with sufficient vertebral surfaces exposed, the same set of homologous feature points were manually identified in the OR using a tracked probe via the Medtronic StealthStation® S7 navigational system (Medtronic Navigation; Louisville, CO). By co-registering the two sets of ordered homologous points in the pCT and the OR coordinate systems, traditional patient registration was established. The registration error for the anatomical landmark patient registration, as reported by the StealthStation, is shown in Table I for each case. The mean estimated registration error was 2.38±0.62 mm.

The coordinate systems and transformations involved in patient registration are illustrated mathematically in Equation 1, and visually in Fig. 1. Specifically, a “world” coordinate system provided by the StealthStation serves as a common reference that determines the spatial positions and orientations of the trackers rigidly fixed to the patient’s vertebra or pelvis and the surgical microscope-stereovision camera assembly (i.e., ${}^{patient}T_{world}$ and ${}^{iSV}T_{world}$, respectively; Fig. 1). In a conventional landmark-based approach for patient registration, the transformation between the patient in the OR and the corresponding pCT image volume (i.e., “patient registration” or ${}^{pCT}T_{world}$ in Fig. 1) is obtained by matching two sets of ordered homologous anatomical markers identified in the OR using a digitizing stylus (typically 8–10) and in the pCT image space. When the spatial transformation between iSV and pCT image volumes (i.e., ${}^{pCT}T_{iSV}$) is directly available, the patient registration (${}^{pCT}T_{patient}$) can be readily computed from

$$ {}^{pCT}T_{patient} = {}^{pCT}T_{iSV} \times {}^{iSV}T_{world} \times \mathrm{inv}({}^{patient}T_{world}) \quad (1) $$

which completes the iSV-based patient registration technique described in this work (Fig. 1).

B. Intraoperative stereovision image acquisition

A custom-designed stereovision system consisting of two C-mount cameras (Flea2 model FL2G-50S5C-C, Point Grey Research Inc., Richmond, BC, Canada) was rigidly mounted to a Zeiss surgical microscope (OPMI® Pentero™, Carl Zeiss, Inc., Oberkochen, Germany) through a binocular port [37]. The cameras were operated at a resolution of 1024×768, and capable of recording 15 fps (frames per second). In this study, however, only a single iSV snapshot was acquired for each camera/microscopic position and orientation. All iSV images were recorded at the same microscopic zoom and focal length to simplify image reconstruction, although an efficient surface reconstruction method at arbitrary camera settings without recalibration does exist [38]. A tracker was rigidly attached to the operating microscope to allow the reconstructed iSV surface to be transformed into the patient's space via the Medtronic StealthStation® S7 navigational system.

For each patient, multiple iSV image pairs (range 3–8) were acquired to ensure sampling of all exposed spinal surfaces. Combining multiple image pairs offers the advantage of increased field-of-view (FOV), which may improve registration performance. However, this requires additional image processing, and, as the number of included vertebrae increases, the distorting effect of patient re-positioning (e.g. supine image acquisition vs. prone surgery) is magnified by accumulation of motion between segments. This effect was observed in patients 2 and 5, both of whom had more than six vertebrae visible within the surgical field (Table I). As a result, we selected only one iSV image pair for each patient registration (which was a direct "top" view sampling 2–3 consecutive vertebral segments).

C. Geometrical surface reconstruction and accuracy assessment

Both stereoscopic camera calibration and correspondence matching between two rectified images are critical for accuracy in iSV surface reconstruction [39], [40]. Techniques for camera calibration are well studied [39]. Here, the stereoscopic system was calibrated prior to surgery using an instrumented calibration block by matching a set of points with known 3D coordinates to their counterparts found in the stereo image pair [23]. A perspective projection matrix was then established from the resulting intrinsic and extrinsic calibration parameters for surface reconstruction, following image rectification and triangulation of correspondence points.

Correspondence matching between two rectified left and right camera images is essentially a nonrigid registration along the epipolar line, which is a constraint established during rectification (Fig. 2a and 2b). Most algorithms are based on optimization of cross-correlation or its variants (e.g., sum of squared differences) between two windowed sub-images [40]. Here, we employed an optical-flow-based technique to treat the correspondence matching as an unconstrained nonrigid registration to obtain a pixel-level disparity map [41]. The full-field disparity maps can be readily used for feature segmentation and assessment of confidence in correspondence matching (see Section II.D for details).

The millimeter accuracy of the iSV system has been previously quantified on a phantom [23], and more recently, on a phantom and neurosurgical patient cases [38]. Similarly in this study, we used a tracked probe to sample selected feature points on the exposed spinal

surface independently by acquiring additional iSV images with the probe in view to minimize localization uncertainty. Their locations were then compared with their homologous points manually identified on the reconstructed iSV surface to report the reconstruction accuracy in terms of point-wise distance error for each patient. Certainly, errors from the probe calibration and landmark localization compromise the accuracy evaluation of the iSV technique. However, the former is sub-millimetric (<0.5mm) and well characterized by the manufacturer. The latter is more difficult to quantify precisely, but is also considered to be small (<1 mm). Thus, despite introducing some errors that bound the accuracy to which the iSV reconstruction can be assessed, the tracked probe is a widely used and well-accepted digitizer that provides a practical reference for comparison within the actual surgical setting, and hence, makes an appropriate, even if imperfect, gold standard.

D. Image preprocessing

To improve registration performance, maximizing the overlapping regions between common features of the exposed bony surfaces in iSV and pCT was necessary. Because the horizontal disparity map resulting from the optical flow was full field, morphological operations (e.g., median filtering to reduce noise) and feature segmentations based on topological information were possible (Fig. 2c). Therefore, the spinous processes were automatically segmented via region growing [42] because they were topologically “above” the surrounding tissue (red boundaries in Fig. 2a and 2c). However, for exposed spinal surfaces on the transverse processes, the height difference in the horizontal disparity map was insufficient for automatic segmentation. Consequently, these areas were manually delineated (green boundaries in Fig. 2a). The vertical disparity map further facilitated the segmentation/delineation of features because of the zero “ground-truth” vertical displacement known *a priori* as a result of the epipolar constraint (i.e., any vertical disparity larger than a threshold would indicate poor confidence in correspondence matching at a particular location; Fig. 2d). Only areas corresponding to actual bony structures were used for registration.

The pCT images were first Gaussian-filtered and then thresholded. Voids in the resulting binary image volume were filled to generate an iso-surface of the spine. Because iSV only captured the exposed surface of the spine, the pCT surface was limited to the dorsal side for registration. This data set was generated by removing pCT iso-surface nodes according to their coordinates and their surface normal directions (i.e., nodal coordinates 3 cm away from the spinal process tip in the ventral direction or nodal surface normals pointing away from the dorsal direction were removed; Fig. 3a).

E. Multi-start patient registration

To improve the point-based registration performance, we employed a variant of the ICP algorithm based on kd-tree search for correspondence point matching with optimized subset selection and minimization techniques [43]. Prior to registration, the reconstructed iSV surface was first transformed into the pCT image space by aligning a pair of homologous points manually identified on the two corresponding surfaces (i.e., “anchor” point pair; e.g., using the tip of a spinous process visible in both iSV and pCT; Fig. 3). However, only aligning the anchor point pair with an arbitrary relative orientation between the two point clouds was not sufficient to ensure a correct registration because ICP algorithms are

sensitive to the initial alignment [29], [30]. Therefore, a classical multi-start registration was employed in which a number of initial starting points (N=16×10=160; fully utilizing a dual octo-core computer; See Section II.G) were generated by randomly rotating the iSV surface in pCT image space while maintaining the anchor point alignment. ICP registrations corresponding to each initial starting point were executed independently but in parallel. Again, because the converged registration may not correspond to the correct one [29], [30], a second pair of homologous points was identified on the iSV and pCT surfaces (i.e., testing point; e.g., using the tip of a different spinous process, preferably far from the anchor points; Fig. 3) to assess the likelihood of registration success. Upon convergence, the registration that resulted in the smallest distance between the testing points was chosen as the final result. The anchor and testing point pairs only needed to be *approximate*; therefore, unlike in the landmark registration, a precise or accurate identification of these points was not necessary. Registrations that resulted in distance errors greater than 10 mm between the testing points were considered failed.

F. Registration accuracy and robustness

Registration accuracy was assessed in terms of average surface-to-surface distance between iSV and pCT point clouds corresponding to the exposed spine after registration convergence. Specifically, for each point in iSV, its closest point on the pCT surface was identified using a kd-tree approach [44]. The average of the resulting point-wise distances were reported to evaluate the registration accuracy.

The robustness of patient registration is important to assess for feasibility and safety in clinical application. Because of the spine's approximate anatomical symmetry in the medial-lateral direction, characterizing the translational and rotational capture ranges along and about each major axis is important. Therefore, the iSV data points were systematically perturbed at regular steps away from their successfully converged locations ("ground-truth"; step size of 1 mm) along and about the three major axes passing through the iSV point cloud centroid. The same ICP registration was launched to reregister the perturbed iSV data and the stationary pCT point cloud. For each perturbation, distances between the newly converged iSV points and their counterparts in the "ground-truth" locations were computed to report an average residual distance error based on point-wise distances. A distance error threshold of 2 mm was used to define a successful registration, and the capture ranges were found as the largest consecutive linear or rotational perturbation about the "ground-truth" position within which the re-registrations were successful.

G. Data analysis

To ensure sufficient resolution in data used for registration while minimizing computational cost, the iSV images were down-sampled to achieve a point cloud resolution (i.e., average closest point distances) of approximately 0.4–0.5 mm. Similarly, the pCT iso-surface was also decimated to produce a resolution of approximately 0.5 mm. The computational cost of iSV surface reconstruction was typically 10 sec. The accuracy of iSV geometrical surface reconstruction was evaluated in terms of average point-wise distances between selected feature points on the exposed spinal surface. For iSV-based patient registration using the ICP algorithm, a point-wise distance error between iSV and pCT was unavailable because

no physical correspondence between feature points existed between the two image-modalities. Instead, the patient registration accuracy was evaluated in terms of average surface-to-surface distance between the two 3D point clouds. To compare with the performance of the anatomical landmark method, the same surface-to-surface distance error (SDE) was reported by using the landmark registration to transform iSV into the pCT image space. The computational cost of the ICP patient registration was also reported (excluding the manual intervention for image segmentation and point pair identification, which were typically completed within 1–2 minutes). Finally, the translational and rotational capture ranges were summarized for each patient along and about each major axis. All image processing and data analyses were performed on a Windows computer with due octo-cores (Intel Xeon E5-2650, 2.6 GHz, 32 GB RAM) using MATLAB (R2014a, The Mathworks, Natick, MA).

III. Results

A. iSV geometrical reconstruction accuracy

The iSV surface reconstruction accuracy in terms of average point-wise distance error is shown in Table II for each patient along with the number of probe points available for accuracy evaluation. The average reconstruction accuracy was 2.21±0.31 mm for the 8 patients based on an average of 5 probe points. Fig. 4 shows the reconstructed iSV surfaces and feature points used for accuracy assessment in 3 patients as illustrative examples.

B. Patient registration accuracy

For each patient, SDE for the iSV patient registration was consistently smaller than the anatomical landmark equivalent, and resulted in a superior accuracy of 1.43±0.35 mm compared to 2.02±0.30 mm (Table II). The average computational cost for iSV patient registration was significantly less, 95.8±48.9 sec (range 33–184 sec), compared to ~30 min for a typical landmark registration involving point identifications in both pCT and in the OR.

Using either landmark or iSV patient registration, the iSV surface was transformed into pCT space and the cross-sections from these surfaces (from landmark and iSV registration) intersecting the corresponding axial pCT image were formed. Contours from the two surfaces were similarly aligned as shown in Fig. 5 for patient 2 and several other patient cases (patients 1, 4 and 6) in Fig. 6, suggesting the registration accuracy is comparable for the techniques.

C. Patient registration robustness

Table III summarizes the translational and rotational capture ranges for each patient. Directional dependency was not evident in the rotational capture ranges. The overall average translational and rotational capture ranges combining all the three directions were 23.8±11.2 mm and 46.0±12.3 deg, respectively. Fig. 7 shows residual errors as a result of the perturbation and re-registration process for a typical patient (patient 2). The translational capture range along the *x* or medial-lateral direction and all of the rotational capture ranges were approximately symmetric relative to the center (i.e., “ground-truth” registration),

whereas symmetry was not evident in the translational capture ranges in the ventral-dorsal and longitudinal directions (*y* and *z* directions, respectively).

IV. Discussion

An accurate, efficient and reliable registration between anatomy in the OR and the pre-operative images is the cornerstone of successful and effective image-guidance. In spinal surgery, having the ability to update this registration may be particularly important because of the significant loads often imparted to the patient; such loads have the potential to result in significant intraoperative movement of the patient's body. While iCT and fluoroscopy may enable a need-based reregistration, their associated radiation exposure limits the update frequency during surgery.

In this study, we used radiation-free intraoperative stereovision (iSV) to accurately register point cloud generated from the reconstructed iSV surface of the exposed spine to that from preoperative CT (pCT), using an improved ICP algorithm. In 8 patient cases undergoing open spinal fusion surgery involving short or long segments of exposed vertebrae (2–3 vs. 6–7 segments, respectively), the iSV patient registration achieved an average accuracy of 1.43±0.35 mm, measured as surface-to-surface distance error (SDE) between the two point clouds. This was consistently smaller than the average SDE from the conventional, anatomical landmark method in every patient case (average accuracy of 2.02±0.30 mm; Table II). While both registration techniques achieved an overall average accuracy within the recommended 2 mm tolerance for spinal procedures [5], errors greater than 2 mm occurred in 3 patients (patients 5, 6, and 8) with landmark registration; additionally, patients 5 and 8 had a Stealth-reported error greater than 3 mm with the conventional patient registration (Table I). By contrast, with the iSV technique, all errors were less than 2mm (Table II).

To some extent, the improved accuracy afforded by iSV was expected - the ICP algorithm is designed to minimize SDE. Nonetheless, comparable accuracy between the two registration approaches was also observed qualitatively by comparing the alignment of vertebral bony features between pCT and the transformed iSV surface using their respective registration (Fig. 5 and 6).

The computational cost of the iSV-based registration was 1.5 min on average (largest of 3 min; Table II), a significant improvement over the landmark registration (typically ~30 min). Although some manual intervention was still needed with the iSV registration, neither accurate feature segmentation nor precise placement of homologous point pairs was necessary to achieve convergence of the multi-start registration. In contrast, accurate and precise identifications of anatomical feature points both in pCT and on the patient were crucial to the accuracy of the landmark registration, which required substantial investment of time and effort on the part of the surgeon. Thus, the benefit of iSV-based spinal registration may reside both in its accuracy and efficiency.

The large overall capture ranges (average of 23.8±11.2 mm in translation and 46.0±12.3 deg in rotation) were comparable to other intramodality volumetric image registrations such as 3D ultrasound (e.g., 32.5 mm in [45] and 40 deg in [46]), suggesting iSV patient registration

may be sufficiently robust in the context of open spinal surgery. Instead of evaluating the translational/rotational directions in sum (common for the brain [46], [47], the heart [48] and abdominal and thoracic organs [45]), we report the capture ranges along and about each major axis separately because of the anatomical symmetry of the spine.

Indeed, the apparent symmetry and asymmetry in the translational and rotational capture ranges (Fig. 7) suggest an anatomically directional dependency in the robustness of the iSV-to-pCT registration, which was expected because of the approximate spine medial-lateral symmetry and the vertebral geometrical similarity along the longitudinal direction. The translational capture range component along the longitudinal direction of the spine is likely to be the most relevant for an actual patient registration because the iSV and pCT point clouds could first be demeaned and pre-aligned in the medial-lateral and ventral-dorsal directions before starting the actual registration process. The smaller translational capture range along the longitudinal direction (15.4±2.1 mm on average; Table III), which presumably is the result of the repetition of morphologically similar vertebral segments. Because the error metric from the ICP algorithm may not reliably identify the desired registration, some *a priori* knowledge of the initial alignment between iSV and pCT may be necessary to ensure a robust registration (e.g., manually identifying at least one “testing point pair”).

To evaluate the significance of inter-operator variability in localizing testing points, their locations in iSV and pCT were randomly perturbed (N = 20; within a radius of 5 mm) for a typical patient (Patient 2). All of the perturbed testing point pairs yielded virtually the same final registration. The relative insensitivity of registration performance to inter-operator variability in the testing point localization was not surprising, given the large capture ranges and the small residual errors for all of the successfully converged registrations (Fig. 7). Certainly, more homologous point pairs (at least 4 point pairs that are not co-linear, and more are usually preferred to increase robustness) could be used to generate an initial registration sufficiently close to the “ground-truth” to enable a “single-start” registration. Although testing points can be eliminated for registration verification, an ordered point-pair list is necessary and would require extra personnel time and effort. Conceptually, the “single-start” approach would degenerate into a probe-based registration, which would defeat the purpose of using the iSV technique to minimize user intervention in the first place. On the other hand, a completely automatic approach may not be desirable clinically, given the catastrophic consequences that could result should misalignment/mis-registration occur during spine surgery.

Both the landmark and iSV patient registrations suffered from the limitation of a one-time rigid registration that does not compensate for intervertebral motion between segments. This limitation could be especially important when many vertebral segments (e.g., >3) are involved because of accumulated motion between vertebral bodies. Incorporating multiple iSV image pairs may address this limitation, for example, by combining multiple iSV surfaces sampling different vertebral bodies into a unified point cloud. The combined iSV surface could then be used to register with pCT using the same multi-start registration technique developed in this study. The resulting rigid registration provides an initial starting position for a second, more refined registration to compensate for intervertebral motion,

possibly without the need of further manual intervention. Because iSV represents the actual spinal geometry during surgery, individual vertebra in pCT may need to be segmented and individually matched with the iSV surface. On the other hand, the registration robustness for an individual vertebra may degrade because of reduced sampling, which, in turn, may adversely affect registration reliability. Alternatively, two or three adjacent vertebrae could be treated as a single unit. This two-step registration strategy is likely feasible, given the registration performance already achieved in this study based on 2–3 segments for each patient. Combining multiple iSV images may also overcome line-of-sight limitations (Fig. 6a). By acquiring images from different perspectives, additional sampling regions from each individual vertebra can be incorporated into the registration process, thereby improving registration robustness and performance.

An important limitation of this study is the lack of a point-wise target registration error (TRE), which was unavailable because no homologous feature points existed between iSV and pCT for these patients. It is possible to instrument fiducial markers on phantoms [22] or animal models that are discretely visible in both iSV and pCT to report point-wise TREs; however, the added invasiveness and risk of additional instrumentation for purely research purposes could not be justified in human patients. Alternatively, intraoperative CT (iCT) may be employed to serve as ground-truth.

The accuracy of the iSV geometrical reconstruction was 2.21±0.31 mm on average, based on point-wise distances between features identified on the surface and their “ground-truth” counterparts reported by the tracked probe, which was comparable to the recommended level of 2 mm in spine surgery [5]. However, these results were not as good as the iSV surface reconstruction accuracy reported for the brain (1.26 mm and 0.71 mm along and perpendicular to the microscope optical axis on patient cases, for an approximate overall accuracy of 1.45 mm; [38]). This reduced reconstruction accuracy can likely be attributed to the more complex topology of the spine, the relatively “feature-less” bony area in terms of image intensity where points were sampled for accuracy assessment (as opposed to the geometrically simpler but feature-rich cortical surface in the brain [35]), and the larger localization error associated with these factors. Despite the challenges, the results presented here provide important initial confidence in the technique which awaits further systematic investigation in the future.

Similarly to any vision-based technique, iSV registration requires sufficient exposure of bony surfaces for geometrical reconstruction, which translates into additional time and effort on the part of the surgeon to remove soft tissues (~5 min for a typical case). The probe-based approach is seemingly insensitive to complete soft tissue removal, but still requires time, effort and experience on the part of the surgeon to define and localize anatomic landmarks. Further, point registration may not be possible later during surgery, for example, after instrumentation or bone removal when anatomical feature points become inaccessible or no longer exist.

Combining the iSV registration technique with other imaging modalities such as ultrasound [19]–[22], [49] may mitigate the requirement of having sufficient bone exposure. Because the two imaging modalities have complementary information and features sampled in the

region of interest (surface only with geometrical information in iSV vs. intensity information capturing surface/subsurface features in ultrasound), a more accurate and robust patient registration is likely to follow than either image modality alone can offer. In addition, the inherently co-registered ultrasound may alleviate some of the manual effort involved in iSV segmentation (e.g., using easily detectable bony features in ultrasound images to aid the segmentation of bony surfaces in iSV), thereby further improving the efficiency and efficacy of image-based patient registration in open spinal surgery.

If an accurate and efficient patient registration can be achieved on-demand with radiation-free intraoperative images, the technique is likely to broaden use of spinal navigation within the surgical community, and expand the applications beyond simple pedicle screw placement to other areas such as tumor resection and deformity correction. In the future, such a scheme may enable the safe use of (semi-)autonomous robots capable of identifying and actively reacting to changes in patient registration during surgery.

V. Conclusion

The current study suggests that iSV may provide rapid and accurate rigid registration in open spinal surgery. The registration accuracy achieved appeared to be consistently superior to the conventional, landmark-based technique in terms of surface-to-surface distance; iSV also appeared to be substantially more time-efficient. Future areas of study may include real-time, non-rigid registration that accounts for intraoperative changes in spinal configuration and the use of other imaging techniques, such as ultrasound, to augment registration accuracy and robustness.

Acknowledgments

The authors are grateful to Dr. Timothy Schaewe for technical assistance on SteathLink and help from the Medtronic Navigation (Louisville, CO).

This work was supported, in part, by the NIH 1R21 NS078607, The Dartmouth Clinical and Translational Science Institute under award number KL2TR001088 from the National Center for Advancing Translational Sciences (NCATS) of the NIH (SJ), and the Dow-Crichlow Award (SSL).

References

1. Cleary K, Peters TM. Image-guided interventions: technology review and clinical applications. Annu Rev Biomed Eng. Aug.2010 12:119–42. [PubMed: 20415592]
2. Jost, GF.; Yonemura, KS.; Von Jako, RA. Intraoperative Imaging and Image-Guided Therapy. In: Jolesz, FA., editor. Intraoperative imaging and image-guided therapy. New York, NY: Springer New York; 2014. p. 613-628.
3. Härtl R, Lam KS, Wang J, Korge A, Kandziora F, Audigé L. Worldwide survey on the use of navigation in spine surgery. World Neurosurg. Jan; 2013 79(1):162–72. [PubMed: 22469525]
4. Deyo RA, Nachemson A, Mirza SK. Spinal-Fusion Surgery—The Case for Restraint. Spine J. 2004; 4:138S–142S.
5. Tjardes T, Shafizadeh S, Rixen D, Paffrath T, Bouillon B, Steinhausen ES, Baethis H. Image-guided spine surgery: state of the art and future directions. Eur Spine J. Jan; 2010 19(1):25–45. [PubMed: 19763640]
6. Parker SL, Amin AG, Santiago-Dieppa D, Liauw JA, Bydon A, Sciubba DM, Wolinsky JP, Gokaslan ZL, Witham TF. Incidence and clinical significance of vascular encroachment resulting

from freehand placement of pedicle screws in the thoracic and lumbar spine. Spine (Phila Pa 1976). 2014; 39(8):683–687. [PubMed: 24480963]

7. Foxx KC, Kwak RC, Latzman JM, Samadani U. A retrospective analsyis of pedicle screws in contact with the great vessels. J Neurosurg Spine. 2010:403–406. [PubMed: 20809738]
8. Pesenti S, Bartoli MA, Blondel B, Peltier E, Adetchessi T, Fuentes S. Endovascular aortic injury repair after thoracic pedicle screw placement. Orthop Traumatol Surg Res. 2014; 100:569–573. [PubMed: 25023930]
9. Holly LT. Image-guided spinal surgery. Int J Med Robot Comput Assist Surg. 2006; 2(January):7–15.
10. Tian NF, Huang QS, Zhou P, Zhou Y, Wu RK, Lou Y, Xu HZ. Pedicle screw insertion accuracy with different assisted methods: a systematic review and meta-analysis of comparative studies. Eur Spine J. Jun; 2011 20(6):846–59. [PubMed: 20862593]
11. Gelalis ID, Paschos NK, Pakos EE, Politis AN, Arnaoutoglou CM, Karageorgos AC, Ploumis A, Xenakis Ta. Accuracy of pedicle screw placement: a systematic review of prospective in vivo studies comparing free hand, fluoroscopy guidance and navigation techniques. Eur Spine J. Feb; 2012 21(2):247–55. [PubMed: 21901328]
12. Tormenti MJ, Kostov DB, Gardner Pa, Kanter AS, Spiro RM, Okonkwo DO. Intraoperative computed tomography image-guided navigation for posterior thoracolumbar spinal instrumentation in spinal deformity surgery. Neurosurg Focus. Mar.2010 28(3):E11. [PubMed: 20192656]
13. Rajasekaran S, Vidyadhara S, Ramesh P, Shetty AP. Randomized clinical study to compare the accuracy of navigated and non-navigated thoracic pedicle screws in deformity correction surgeries. Spine (Phila Pa 1976). 2007; 32(2):E56–E64. [PubMed: 17224800]
14. Roessler K, Ungersboeck K, Dietrich W, Aichholzer M, Hittmeir K, Matula C, Czech T, Koos W. Frameless stereotactic guided neurosurgery: clinical experience with an infrared based pointer device navigation system. Acta Neurochir. 1997; 139(6):551–559. [PubMed: 9248590]
15. Brodwater B, Roberts D, Nakajima T, Friets E, Strohbehn J. Extracranial application of the frameless stereotactic operating microscope: experience with lumbar spine. Neurosurgery. 1993; 32(2):209–213. [PubMed: 8437658]
16. Nottmeier EW. A review of image-guided spinal surgery. J Neurosurg Sci. 2012; 56:35–47. [PubMed: 22415381]
17. Ionescu G, Lavallée S, Demongeot J. Automated registration of ultrasound with CT images: application to computer assisted prostate radiotherapy and orthopedics. MICCAI. 1999:768–778.
18. Muratore D, Russ J, Dawant B, Galloway RJ. Three-dimensional image registration of phantom vertebrae for image-guided surgery: a preliminary study. Comput Aided Surg. 2002; 7:342–352. [PubMed: 12731097]
19. Winter S, Brendel B, Pechlivanis I, Schmieder K, Igel C. Registration of CT and intraoperative 3-D ultrasound images of the spine using evolutionary and gradient-based methods. IEEE Trans Evol Comput. 2008; 12(3):284–296.
20. Lang A, Mousavi P, Gill S, Fichtinger G, Abolmaesumi P. Multi-modal registration of speckle-tracked freehand 3D ultrasound to CT in the lumbar spine. Med Image Anal. Apr; 2012 16(3): 675–86. [PubMed: 21982123]
21. Gill S, Abolmaesumi P, Fichtinger G, Boisvert J, Pichora D, Borshneck D, Mousavi P. Biomechanically constrained groupwise ultrasound to CT registration of the lumbar spine. Med Image Anal. Apr; 2012 16(3):662–74. [PubMed: 21126904]
22. Yan CXB, Goulet B, Chen SJS, Tampieri D, Collins DL. Validation of automated ultrasound-CT registration of vertebrae. Int J Comput Assist Radiol Surg. Jul; 2012 7(4):601–10. [PubMed: 22113426]
23. Sun H, Member S, Lunn KE, Farid H, Wu Z, Roberts DW, Hartov A, Paulsen KD. Stereopsis-Guided Brain Shift Compensation. IEEE Trans Med Imaging. 2005; 24(8):1039–1052. [PubMed: 16092335]
24. Paul P, Morandi X, Jannin P. A surface registration method for quantification of intraoperative brain deformations in image-guided neurosurgery. IEEE Trans Inf Technol Biomed. Dec; 2009 13(6):976–83. [PubMed: 19546046]

25. Delorenzo C, Papademetris X, Staib LH, Vives KP, Spencer DD, Duncan JS. Image-guided intraoperative cortical deformation recovery using game theory: application to neocortical epilepsy surgery. IEEE Trans Med Imaging. Mar; 2010 29(2):322–38. [PubMed: 20129844]
26. Miga MI, Sinha TK, Cash DM, Galloway RL, Weil RJ. Cortical surface registration for image-guided neurosurgery using laser-range scanning. IEEE Trans Med Imaging. Aug; 2003 22(8):973–85. [PubMed: 12906252]
27. Ding S, Miga MI, Pheiffer TS, Simpson AL, Thompson RC, Dawant BM. Tracking of vessels in intra-operative microscope video sequences for cortical displacement estimation. IEEE Trans Biomed Eng. Jul; 2011 58(7):1985–93. [PubMed: 21317077]
28. Simpson AL, Sun K, Pheiffer TS, Rucker DC, Sills AK, Thompson RC, Miga MI. Evaluation of conoscopic holography for estimating tumor resection cavities in model-based image-guided neurosurgery. IEEE Trans Biomed Eng. Jun; 2014 61(6):1833–43. [PubMed: 24845293]
29. Besl PJ, McKay ND. A method for registration of 3-D shapes. IEEE Trans Pattern Anal Mach Intell. 1992; 14(2):239–256.
30. Rusinkiewicz S, Levoy M. Efficient variants of the ICP algorithm. Proc Third Int Conf 3-D Digit Imaging Model. :145–152.
31. Mirota DJ, Ishii M, Hager GD. Vision-based navigation in image-guided interventions. Annu Rev Biomed Eng. Aug.2011 13:297–319. [PubMed: 21568713]
32. DeLorenzo C, Papademetris X, Wu K, Vives KP, Spencer D, Duncan JS. Nonrigid 3D brain registration using intensity/feature information. Med Image Comput Comput Assist Interv. Jan; 2006 9(Pt 1):932–9. [PubMed: 17354980]
33. Fan X, Ji S, Hartov A, Roberts DW, Paulsen KD. Stereovision to MR image registration for cortical surface displacement mapping to enhance image-guided neurosurgery. Med Phys. 2014
34. Sinha TK, Dawant BM, Duay V, Cash DM, Weil RJ, Thompson RC, Weaver KD, Miga MI. A method to track cortical surface deformations using a laser range scanner. IEEE Trans Med Imaging. Jun; 2005 24(6):767–81. [PubMed: 15959938]
35. Ji S, Fan X, Roberts DW, Hartov A, Paulsen KD. Cortical surface shift estimation using stereovision and optical flow motion tracking via projection image registration. Med Image Anal. Jul; 2014 18(7):1169–1183. [PubMed: 25077845]
36. Fan X, Ji S, Hartov A, Roberts D, Paulsen K. Registering stereovision surface with preoperative magnetic resonance images for brain shift compensation. Proc of SPIE, Medical Imaging 2012: Visualization, Image-Guided Procedures, and Modeling. 2012; 8316
37. Ji S, Fan X, Fontaine K, Hartov A, Roberts D, Paulsen K. An integrated model-based neurosurgical guidance system. Medical Imaging 2010: Visualization, Image-Guided Procedures, and Modeling. 2010
38. Ji S, Fan X, Roberts DW, Paulsen KD. Efficient Stereo Image Geometrical Reconstruction at Arbitrary Camera Settings from a Single Calibration. MICCAI. 2014:440–447. [PubMed: 25333148]
39. Hemayed, EE. A survey of camera self-calibration. Proc. IEEE Conf. Adv. Video Signal Based Surveillance; 2003; 2003. p. 351-357.
40. Hu X, Mordohai P. A Quantitative Evaluation of Confidence Measures for Stereo Vision. IEEE Trans Pattern Anal Mach Intell. Jan; 2012 34(11):2121–2133. [PubMed: 22331856]
41. Ji S, Fan X, Roberts DW, Hartov A, Paulsen KD. Flow-Based Correspondence Matching in Stereovision. Machine Learning in Medical Imaging. 2013:107–114.
42. Pratt, WK. Digital Image Processing. 4. Los Altos, California: John Wiley & Sons, Inc; 2007.
43. Kjer, HM.; Wilm, J. Evaluation of surface registration algorithms for PET motion correction. Technical University of Denmark; 2010.
44. Bentley JL. Multidimensional binary search trees used for associative searching. Commun ACM. Sep; 1975 18(9):509–517.
45. Shekhar R, Zagrodsky V. Mutual information-based rigid and nonrigid registration of ultrasound volumes. IEEE Trans Med Imaging. Jan; 2002 21(1):9–22. [PubMed: 11838664]
46. Slomka PJ, Mandel J, Downey D, Fenster A. Evaluation of voxel-based registration of 3-D power Doppler ultrasound and 3-D magnetic resonance angiographic images of carotid arteries. Ultrasound Med Biol. 2001; 27(7):945–955. [PubMed: 11476929]

47. Ji S, Wu Z, Hartov A, Roberts DW, Paulsen KD. Mutual-information-based image to patient re-registration using intraoperative ultrasound in image-guided neurosurgery. Med Phys. 2008; 35(10):4612. [PubMed: 18975707]

48. Walimbe V, Zagrodsky V, Raja S, Jaber Wa, DiFilippo FP, Garcia MJ, Brunken RC, Thomas JD, Shekhar R. Mutual information-based multimodality registration of cardiac ultrasound and SPECT images: a preliminary investigation. Int J Cardiovasc Imaging. Dec; 2003 19(6):483–94. [PubMed: 14690187]

49. Ji S, Roberts DW, Hartov A, Paulsen KD. Intraoperative patient registration using volumetric true 3D ultrasound without fiducials. Med Phys. Dec; 2012 39(12):7540–52. [PubMed: 23231302]

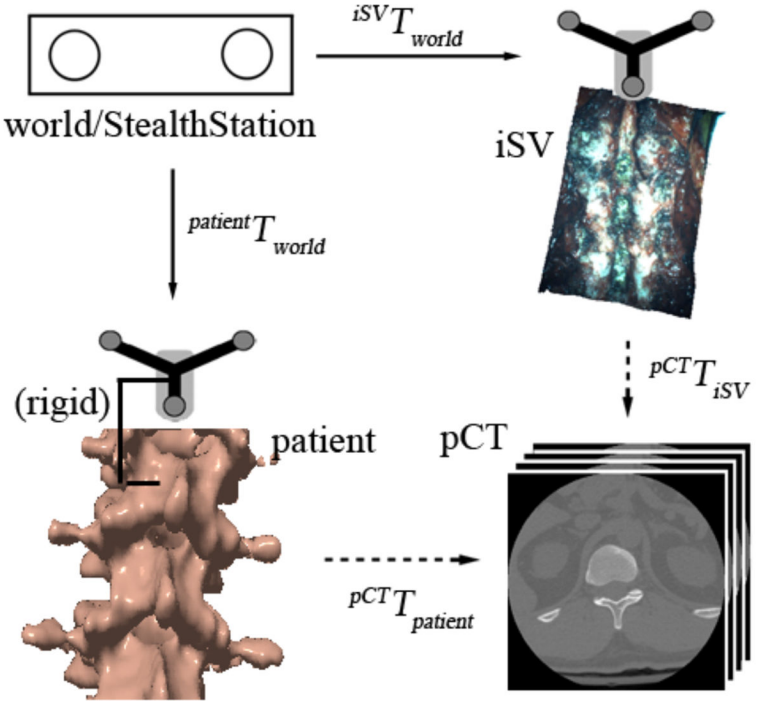

Fig. 1.

Coordinate systems involved in patient registration. Solid/dashed arrows indicate transformations determined from calibration/registration. A transformation reversing the arrow direction is obtained by matrix inversion.

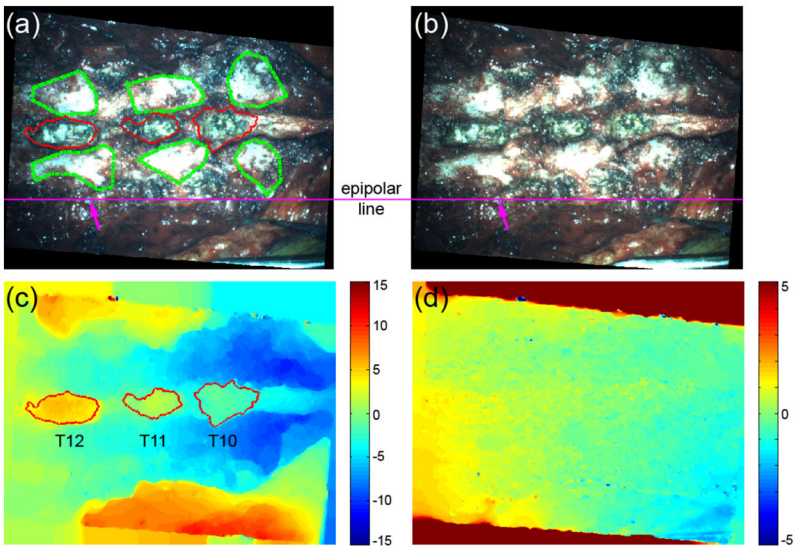

Fig. 2.

The rectified (a) left and (b) right images of the spine for patient 2 and the resulting (c) horizontal and (d) vertical disparity maps. The spinous processes were automatically segmented via a region growing approach based on the horizontal disparity map (red boundaries in (a) and (c)), while other bony areas on the transverse processes were manually delineated (green boundaries in (a)). (d) The vertical disparity map indicates the confidence in correspondence matching as a result of the epipolar constraint. A typical epipolar line is shown in (a) and (b), demonstrating homologous features are aligned on the same horizontal line (arrows; i.e., “ground-truth” vertical disparity of zero). Units in pixels (images down-sampled to 25% along each dimension for illustration).

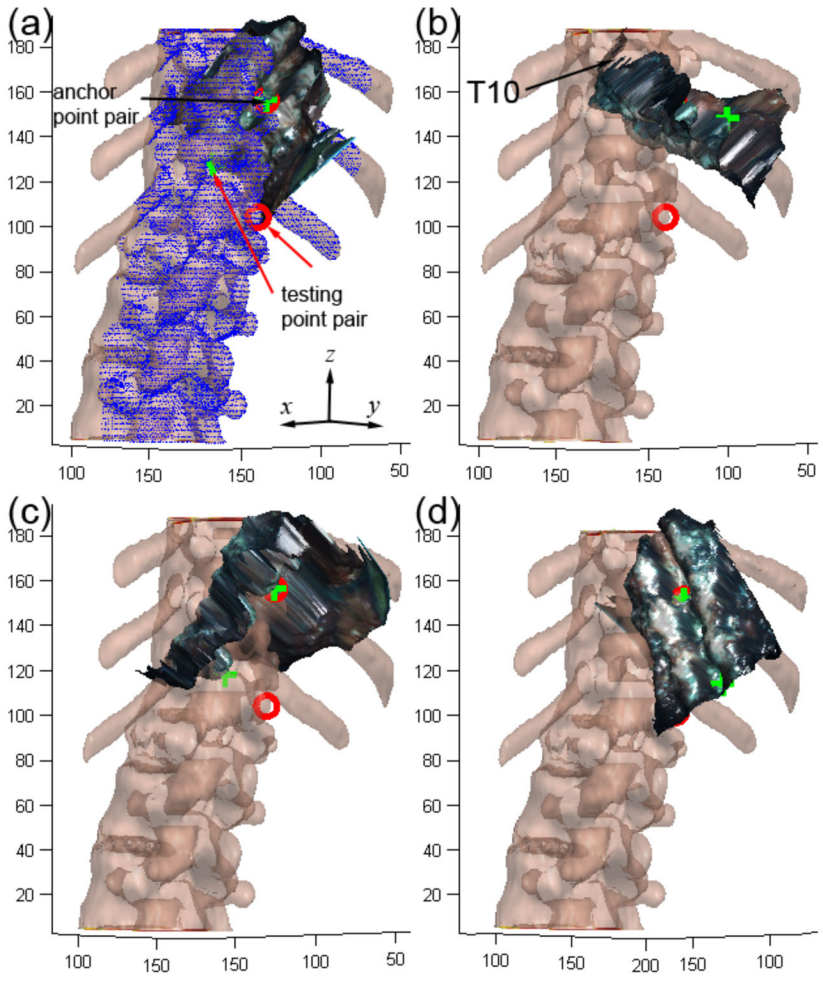

Fig. 3.

(a–d) Illustration of four randomly generated initial starting points used to initiate the multi-start patient registration between iSV and pCT point clouds. Two corresponding point pairs were first manually identified in iSV (green) and pCT (red) to serve as the anchor and testing point pair, respectively. All initial starting points had the anchor point pair pre-aligned as shown in (a). Selected points on the pCT spinal surface used for registration are shown in blue (a).

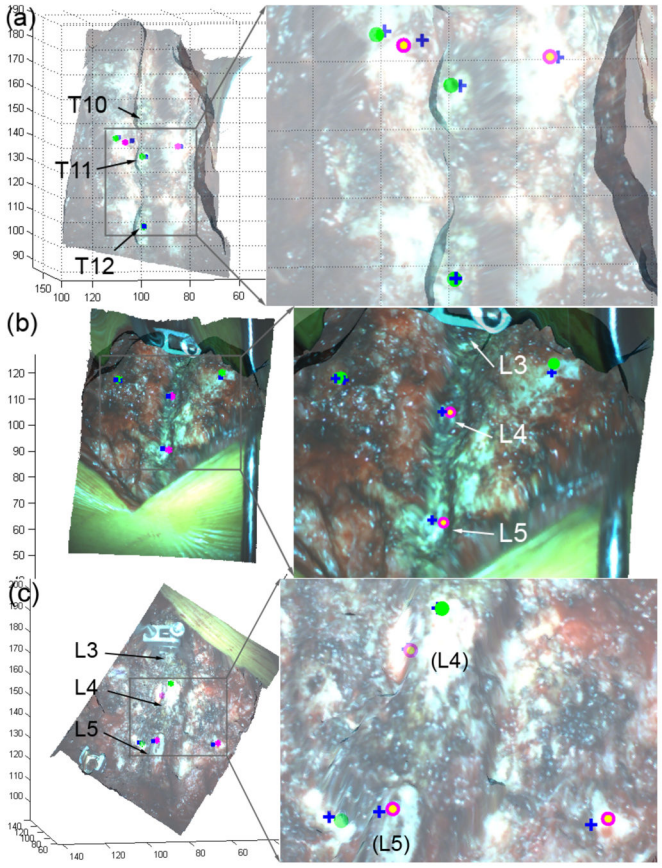

Fig. 4.

(a–c) Reconstructed iSV surface in pCT space for patients 2, 4, and 6, respectively. A set of feature points was identified using a tracked probe (blue crosses). The corresponding homologous locations on the reconstructed iSV surface are also indicated as solid green (relative point-wise distance error = 2 mm) or open magenta (distance error > 2 mm) markers. All units in mm.

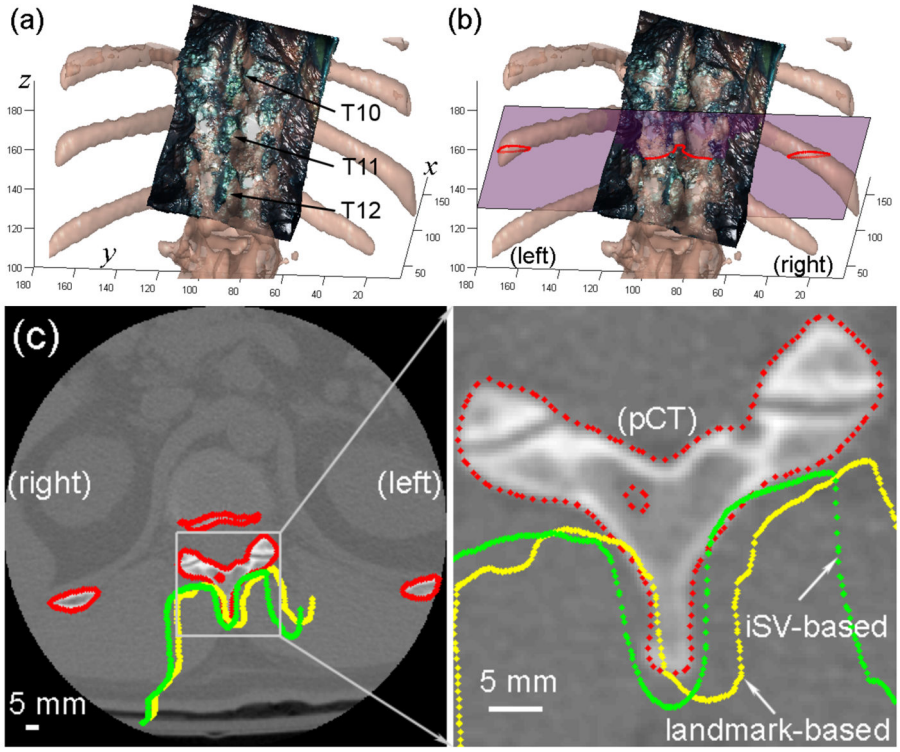

Fig. 5.

Comparison of the alignment between iSV and pCT surfaces using (a) anatomical landmark or (b) iSV patient registration for patient 2. The cross-sections of the pCT surface (red) and those of the iSV surfaces obtained from the landmark (yellow) or iSV (green) registrations are shown on an axial pCT image (the corresponding plane is shown in (b)). Axis units in mm.

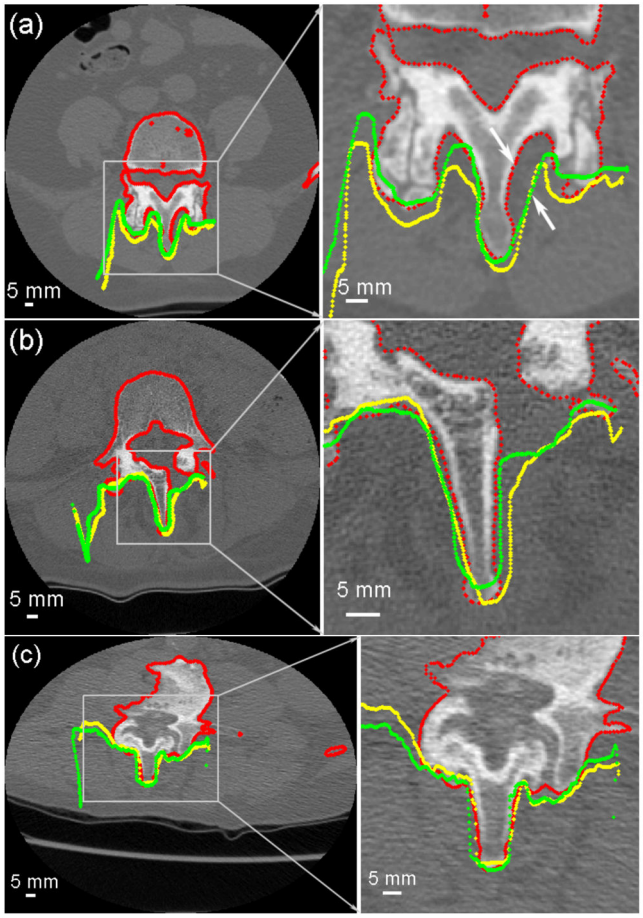

Fig. 6.

(a–c) Cross-sections of the segmented pCT surface (red) overlaid with the reconstructed iSV surfaces obtained from the landmark (yellow) or iSV (green) registrations for patients 1, 4, and 6, respectively. The large mismatch between iSV and pCT surfaces in (a) resulted from incomplete iSV sampling due to its line-of-sight limitations (see arrows).

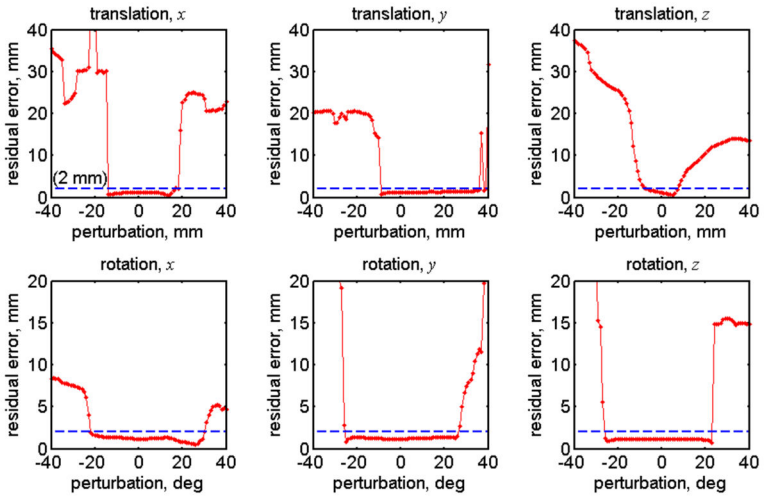

Fig. 7.

Residual errors as a result of perturbation and re-registration between iSV and pCT point clouds to estimate the translational and rotational capture ranges for a typical patient case (patient 2). The approximate symmetry (translation along *x* direction and rotations about *x*, *y* and *z* directions) and asymmetry of the capture ranges (translations along *y* and *z* directions) about the center are evident.

TABLE 1

SUMMARY OF PATIENT GENDER, AGE, CONDITION, STATUS OF PREVIOUS SURGERY, TYPE OF SURGERY, AND THE EXPOSED VERTEBRAE LEVELS (THE TOTAL NUMBER OF VERTEBRAL SEGMENTS EXPOSED ARE SHOWN IN PARENTHESIS). THE ESTIMATED REGISTRATION ERROR REPORTED FROM THE STEALTHSTATION USING THE POINT-WISE LANDMARK APPROACH IS ALSO SHOWN.

Patient (gender/age)	Condition	Previous surgery with bone removed?	Type of surgery	Exposed vertebrae	S7 Registration error (mm)
1 (M/76)	L3–5 stenosis with L4–5 spondylolisthesis	No	L3–5 laminectomy and L4–5 instrumented fusion	L3–L5 (3)	1.65
2 (M/29)	L1 fracture	No	T12-L2 laminectomy and T10-L3 instrumented fusion	T10–T12, L1–L3 (6)	2.16
3 (F/50)	L4–5 spondylolisthesis	No	L4–5 instrumented fusion	L4, L5 (2)	2.76
4 (F/67)	L4–5 spondylolisthesis (prior L4–5 hemilaminotomies)	Yes[1]	L4–5 instrumented fusion	L3–L5 (3)	2.29
5 (M/44)	T6 fracture	No	T3–T8 instrumented fusion	T2–T8 (7)	3.08
6 (M/69)	L2–4 stenosis and scoliosis	Yes[2]	L2–5 laminectomy and instrumented fusion	L1–L3 (3)	1.65
7 (M/64)	L4–5 spondylolisthesis	No	L4–5 instrumented fusion with interbody cage	L3–L5 (3)	2.15
8 (F/61)	L5–L6 spondylolisthesis (supranumerary lumbar vertebra)	No	L5–6 instrumented fusion with interbody cage	L5, L6 (2)	3.31

[1] Prior L4–5 hemilaminotomies;

[2] Prior L4–5 laminectomy and instrumented fusion

TABLE II

SUMMARY OF ISV SURFACE RECONSTRUCTION AND PATIENT REGISTRATION ACCURACIES USING LANDMARK AND ISV TECHNIQUES. THE COMPUTATIONAL COST FOR MULTI-START ISV REGISTRATION IS ALSO INCLUDED.

Pat. #	iSV reconstruction		Registration accuracy (mm)[3]		iSV registration cost (sec)
	# of probe data	Accuracy (mm)[2]	Landmark	iSV-based	
1	4	2.50±1.12	1.95±1.25	1.27±0.91	33
2	5	2.22±1.03	1.83±1.50	1.09±0.73	94
3	4	2.38±0.99	1.93±1.30	1.20±0.77	134
4	5	1.73±0.44	1.73±0.11	1.11±0.61	106
5	8	2.64±1.12	2.71±1.80	1.90±1.41	73
6	5	1.94±0.89	2.01±1.62	1.91±1.82	100
7	4	2.45±0.51	1.98±1.03	1.70±1.12	42
8	6	2.10±1.00	2.03±1.7	1.30±1.02	184
Avg.	5[1]	2.21±0.31	2.02±0.30	1.43±0.35	95.8±48.9

[1] Median value;

[2] iSV reconstruction accuracy is the average point-wise distance error relative to the probe points;

[3] Registration accuracy is the average SDE relative to pCT

IEEE Trans Biomed Eng. Author manuscript; available in PMC 2016 September 01.

TABLE III

SUMMARY OF TRANSLATIONAL (TX, TY AND TZ; IN MM) AND ROTATIONAL (RX, RY AND RZ; IN DEG) CAPTURE RANGES FOR EACH PATIENT CASE.

Pat. #	Tx	Ty	Tz	Rx	Ry	Rz
1	11	22	17	30	21	41
2	30	45	14	51	51	49
3	13	30	16	38	62	47
8	17	29	14	41	61	46
5	29	37	13	28	44	36
6	27	36	13	51	24	56
7	27	55	18	41	71	55
8	18	23	18	49	56	55
Avg.	21.5 ±7.6	34.6 ±11.2	15.4 ±2.1	41.1 ±9.0	48.8 ±18.1	48.1 ±7.2

The *x*, *y*, and *z* directions corresponded to the medial-lateral, ventral-dorsal, and the longitudinal directions of the spine, respectively.

IEEE Trans Biomed Eng. Author manuscript; available in PMC 2016 September 01.